Proceeding of the 2004 American Control Conference
Boston, Massachusetts June 30 - July 2, 2004

Design and Analysis of a Dual-Stage Disk Drive Servo System Using an Instrumented Suspension

Xinghui Huang, Ryozo Nagamune, Roberto Horowitz and Yunfeng Li

Abstract— **This paper presents the design and analysis of a track-following controller using a mixed-objective optimization technique for dual-stage servo systems in hard disk drives (HDD). The objective of minimizing tracking error in the presence of plant uncertainties and operational variations is formulated into a framework of multi-objective minimization. The tracking error minimization is reasonably formulated as an H_2 norm minimization problem, while the robust stability issue is addressed by some H_∞ norm bounds. These norm minimization or constraints are then translated into a set of parametric feasibility conditions using linear matrix inequalities (LMI) which are readily solved by convex optimization solvers. To enhance tracking performance and stability robustness, attenuation of airflow excited suspension structural vibration is also explicitly taken into consideration by an inner-loop fast-rate damping and compensation controller utilizing a vibration sensor on the suspension surface. Analysis and simulation results show a noticeable improvement in tracking performance over a previous designs, while retaining acceptable robust stability under certain multiplicative and parameter uncertainties.**

I. Introduction

Dual-stage actuation, which combines a normal voice coil motor (VCM) actuator and a secondary microactuator (MA) placed close to the head, has been studied intensively as a means of achieving higher track densities, hence higher data capacity in HDDs, by increasing the servo bandwidth. The design and optimization of track-following controllers have been studied by many researchers over the past years. These works vary from decoupled or sequential single-input-single-output (SISO) classical frequency shaping design techniques, such as the master-slave method [1], the PQ method [2], and the sensitivity transfer function decoupling method [3], to those methodologies that explicitly account for the coupling effects between the VCM and MA actuators and that utilize multivariable optimal control design techniques, such as LQG/LTR [4], μ-synthesis [5]. Most of those works optimize the performance by modelling the system in detail and the information of various sources of disturbances is also brought into consideration. A problem related to detailed parametric modelling is stability robustness. Plant uncertainties or variations may deteriorate the claimed performance through detailed parametric modelling. In the worst case, the system may be unstable. A disk servo controller should perform well to meet performance specifications over a huge batch of production drives while providing internal stability under plant uncertainties and operational variations from drive to drive. The μ-synthesis technique incorporates stability robustness in design explicitly through properly modelled uncertainty dynamics or estimated parametric uncertainties. Other design methodologies can only consider robustness implicitly when optimizing system performance.

In this paper, we discuss an optimization method for the dual-stage track-following controller design in hard disk drives. This design methodology formulates multiple objectives as a problem of some norm optimization or norm constraints that can be expressed as a set of LMIs, which are then solved through convex optimization. Quantitative information on the track runout spectrum and on the windage to suspension structural vibrations, and also plant uncertainties are accounted for explicitly in this design. In the context of disk drive servo design, this design methodology was first applied in [6] for a single-stage system. The design presented in this paper is for a dual-stage servo system with a secondary MEMS MA located between the suspension tip and the slider. Realistic models for the VCM, MA, windage, and track runout, are obtained from either experimental tests or finite element analysis. Furthermore, airflow excited structural vibration attenuation is explicitly accounted for by an inner-loop damping and compensation controller, utilizing a strain sensor signal from the suspension surface. This inner controller can be run at a higher rate than that of the basic servo loop since, unlike the position error signal (PES), this strain signal does not have such a physical limitation on its sampling rate. Some distinct issues on robust stability arising from the dual-stage configuration are circumvented properly. Meanwhile, an improved algorithm of norm characterization and controller parametrization has been employed in this design which exhibits less conservativeness and is expected to yield better overall performance [7] over the original algorithm [8].

This paper is organized as follows: Section 2 describes the problem formulation and controller design of the dual-stage servo system. Simulation results and analyses are presented in Section 3. Section 4 concludes this paper.

II. Multi-Objective Track-Following Control Design

The dual-stage servo system consists of two actuators: a main VCM actuator, and a secondary actuator MEMS MA,

This work was supported by the Information Storage Industry Consortium (INSIC) and the Computer Mechanics Laboratory (CML) of U.C. Berkeley.

X. Huang, R. Nagamune and R. Horowitz are with the Department of Mechanical Engineering, U.C. Berkeley, CA 94720 {xhhuang, ryozo, horowitz}@me.berkeley.edu.

Y. Li is with the Maxtor Corporation, 500 McCarthy Blvd, Milpitas, CA 95035, yunfeng_li@maxtor.com.

0-7803-8335-4/04/$17.00 ©2004 AACC

which is sandwiched between the gimbal and the slider. It can generate translational motion of the slider relative to the suspension tip and therefore provide the potential for achieving higher servo bandwidth. The magnitude frequency responses of the VCM and MEMS MA are shown in Fig. 1. With proper design and assembling, the MEMS MA has a moderately damped resonance mode around 2 kHz and no other appreciable structural resonance modes up to 40 kHz. Therefore, it can be modelled as a simple mass-spring-damper second-order system. Capacitive sensing can be incorporated into the MA such that the relative motion output of the MA, $RPES$, can be measured. On the other hand, an 8th-order model is used for G_V in order to capture the suspension's major structural vibration modes, as they become more important for the targeted 3-σ tracking precision of 5 nm. We also assume that strain gauges will be attached to the surface of the suspension such that suspension vibration information can be detected for inner loop vibration control [9][10]. Ideally, one wants the sensors to be sensitive to only those vibration modes that generate off-track motions of the read/write head while be able to reject other irrelevant modes. As in the case of the $RPES$ signal, there is also no limitation on the sampling rate of the strain gauge output, y_{PZT}, and the vibration control loop is able to be run at a higher rate than the PES feedback loop to achieve better vibration control.

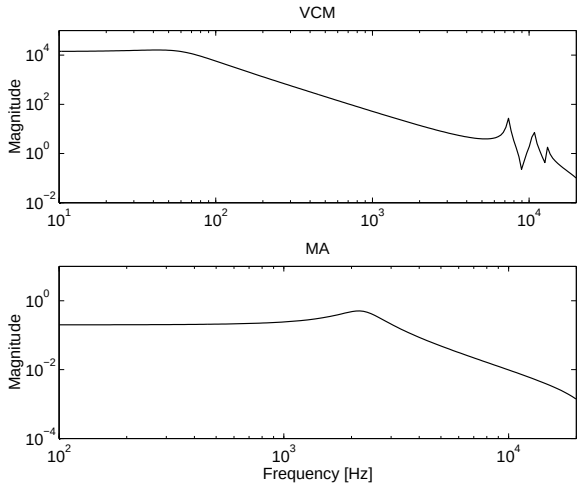

Fig. 1. Magnitude-frequency responses of VCM and MEMS MA.

A. MA RPES Minor Loop Damping Controller Design

Before designing the vibration and outer loop tracking controllers, it is necessary to first design the MA inner loop controller, by using the $RPES$ signal so that the MA's single resonance mode around 2 kHz is adequately damped. This damping is critical to the design that follows and its effectiveness will be shown in the simulation results later on.

The MA dynamics is described by a mass-spring-damper second-order transfer function:

$$G_M(s) = \frac{A_M}{s^2 + 2\zeta_{MO}\omega_{MO}s + \omega_{MO}^2}\,. \tag{1}$$

Its zeroth-order-hold discrete-time transfer function is

$$G_M(q^{-1}) = \frac{q^{-1}B_o(q^{-1})}{A_o(q^{-1})}\,, \tag{2}$$

where q^{-1} is the one-step delay operator. The MA damping loop is illustrated in the lower part of Fig. 2. With pole placement, the closed-loop transfer function G_R can be expressed as

$$G_R(q^{-1}) = \frac{q^{-1}B_o(q^{-1})}{A_R(q^{-1})}\,. \tag{3}$$

This can be achieved by solving the following Diophantine equation

$$A_R(q^{-1}) = A_o(q^{-1})K_{RS}(q^{-1}) + q^{-1}B_o(q^{-1})K_{RR}(q^{-1})\,. \tag{4}$$

The closed-loop polynomial $A_R(q^{-1})$ is chosen by the designer and its roots are the damped MA poles. Normally the damping ratio for G_R to set to be equal to 1.

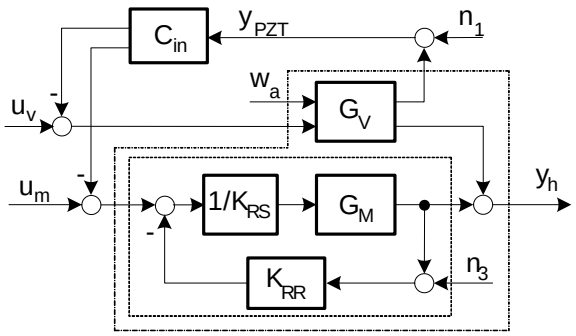

Fig. 2. Block diagram of MA inner loop damping and suspension vibration damping and compensation.

B. Vibration Damping and Compensation Control Design

After the minor loop around MA is closed, the vibration damping and compensation controller, C_{in}, is designed using y_{PZT}, which provides vibration information of the suspension. The design of the inner loop controller is formulated as a standard LQG problem. Consider the discrete-time representation of plant that incorporates the MA inner loop damping, which is shown in the outer frame with dashed line in Fig. 2:

$$\begin{aligned} x(k+1) &= Ax(k) + Bu(k) + B_w w_a(k) \\ y(k) &= Cx(k) + n(k) \end{aligned} \tag{5}$$

where $y(k) = [y_h(k)\ y_{PZT}(k)]^T$, $u(k) = [u_v(k)\ u_m(k)]^T$, and the airflow turbulence $w_a(k)$ to the suspension and the measurement noise $n(k)$ are assumed to be random sequences with zero mean. The goal of the inner controller design is to minimize the cost function

$$J = E\left\{y_h^2(k) + Ru^2(k)\right\} \tag{6}$$

where $E\{\cdot\}$ is the expectation operator, and the control penalty matrix R is given by $R = \text{diag}(r_v,\ r_m)$ with r_v and r_m being the penalties on the control inputs, u_v and u_m, respectively. The VCM vibration suppression controller acts by actively damping off-track suspension vibration modes, while the MA vibration suppression controller acts producing a MA motion that compensates airflow-induced suspension vibration off-track motion at its tip. Figs. 3 and 4 show the magnitude responses of the plant when the vibration damping and compensation controllers are closed. Two sets of input weight R were used in the simulation study. The first set, which will be referred to as weight set (a), is given by $R = \text{diag}(0.6,\ 3)$, while the second, which will be referred to as weight set (b), is given by $R = \text{diag}(6,\ 3)$. Notice that weight set (b) has a higher relative VCM control input weighting than weight set (a). In the figures, the dotted curve show the read/write head position response without vibration control, while the solid curve show the read/write head position when the vibration controller is closed. Also shown in the figures are the frequency responses of the suspension tip output (dashed curve) and the MA relative motion output, $RPES$ (dash-dotted curves). It can be seen in the two figures that the VCM provides a higher degree of active damping control in Fig. 3 than in Fig. 4, where more penalty on the VCM control effort was used in the cost function in Eq. (6). Conversely, the MA actuator provides a higher degree of feedforward compensation motion in Fig. 4.

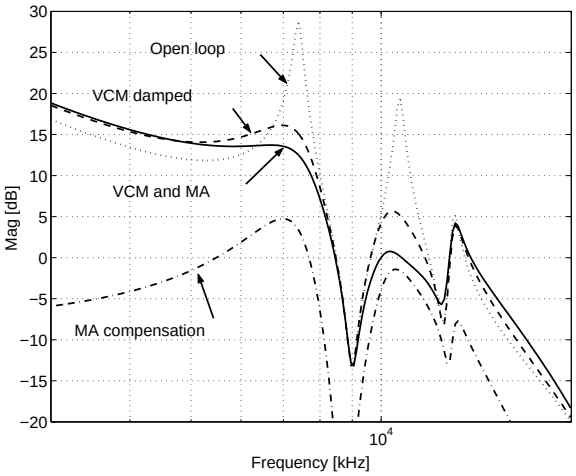

Fig. 3. Magnitude-frequency response of VCM actuator with and without inner loop damping for weight set (a).

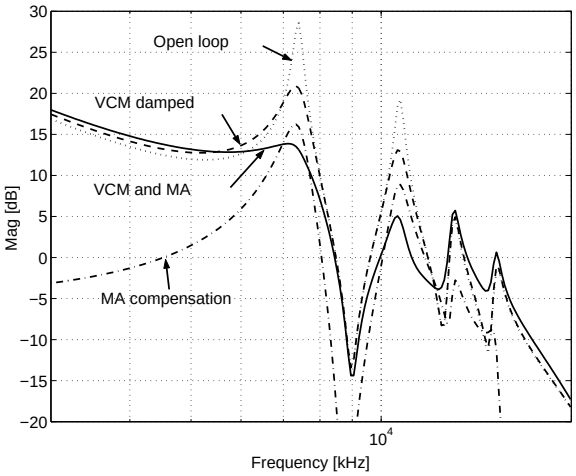

Fig. 4. Magnitude-frequency response of VCM actuator with and without inner loop damping for weight set (b).

C. Outer Loop Track-Following Control Design

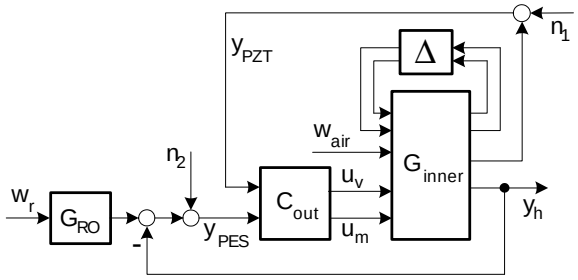

Fig. 5. Block diagram of the outer loop tracking control system

Fig. 5 shows the block diagram of the track-following control system. In the figure, G_{inner} is the general plant shown in Fig. 2, in which the minor loop damping around MA and suspension vibration attenuation control loop around both VCM and MA have been incorporated. Track runout is generated by the normalized white signal w_r through the frequency shaping function G_{RO}. Airflow disturbance w_a and measurement noises, n_1 and n_2, are also considered. The goal of tracking control design is to achieve optimal performance while retaining robust stability over parameter variations and unmodelled dynamics. This objective is approached by multi-objective optimization technique via the solution of LMIs and will be detailed in the following subsections.

1) Tracking error minimization: The main objective of the HDD's servo system is to make the position error signal, PES, as small as possible, in order to achieve high areal density and low readout error rate. Since the entire system is adequately modelled as a stochastic system, i.e., all external disturbances can be considered as random signals with Gaussian distribution, the tracking performance is normally characterized by the 3σ-value of the PES. When all the disturbance sources are normalized through proper weighting functions, minimizing this RMS value is then equivalent to minimizing the H_2 norm of the transfer function from those normalized disturbances to the PES, i.e.,

$$\min_{\mathcal{C}} \text{RMS}\left(PES(t)\right) \ \Leftrightarrow\ \min_{\mathcal{C}} \|G_{z_2 w_2}\|_2\,, \qquad (7)$$

where $z_2 := PES$ and $w_2 := [w_r, w_a, n_1, n_2]^T$.

2) Stability robustness: Stability robustness is an important issue for practical implementation of hard disk servo controllers since there always exist uncertainties and variations in disk drive plant dynamics. It is infeasible to fine tune controller parameters with respect to each individual disk drive and working conditions. Therefore, the designed controller should retain stability over a batch of drives, that is, should exhibit stability robustness. To this end, both qualitative and quantitative information about plant uncertainties should be known to some extent and be brought into consideration during the design process. There are three main ways of representing uncertainties and parameter variations: parametric uncertainty, multiplicative uncertainty and additive uncertainty. To apply the controller synthesis results via LMIs, one needs to address stability robustness by imposing bounds on the H_∞ norms of some appropriately chosen transfer functions. It is therefore easier to model uncertain dynamics as multiplicative uncertainties. That is, the actual plant dynamics are expressed as

$$G_V(s) = G_{V\mathrm{nom}}(1 + \Delta_V(s)W_V(s))\,, \tag{8}$$

$$G_M(s) = G_{M\mathrm{nom}}(1 + \Delta_M(s)W_M(s))\,, \tag{9}$$

where $||\Delta_V||_\infty \leq 1$, $||\Delta_M||_\infty \leq 1$. Fig. 6 shows candidate uncertainties used in the simulation.

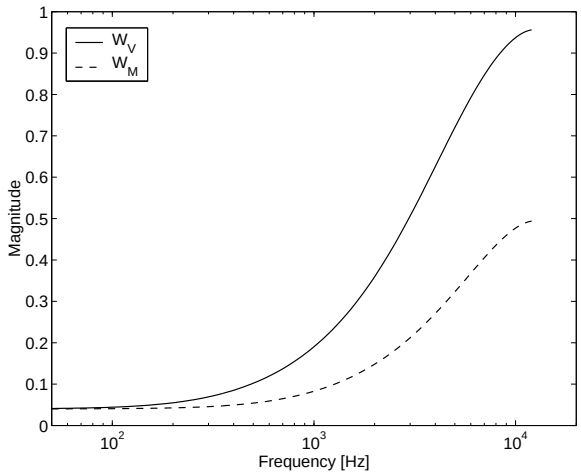

Fig. 6. Uncertainty weighting functions W_V and W_M.

Assuming multiplicative uncertainties, the uncertain block Δ shown in Fig. 5 becomes a diagonal block with

$$\Delta = \begin{bmatrix} \Delta_V & 0 \\ 0 & \Delta_M \end{bmatrix} \text{ and } \sup_\omega \bar{\sigma}(\Delta\,(j\omega)) \leq 1\,. \tag{10}$$

When plant uncertainties are modelled as multiple parametric uncertainties, the system's stability robustness is more precisely characterized by the structured singular value, $\mu_\Delta(G(j\omega))$, rather than its H_∞ norm, which is normally excessively conservative.

From the μ-theory [11], it is well known that given condition (10), the closed-loop system retains internal stability if and only if

$$\sup_\omega \mu_\Delta\,(G_{\mathrm{cl}}(j\omega)) < 1\,. \tag{11}$$

This μ-value is in general smaller than $\|G_{\mathrm{cl}}\|_\infty$ when Δ is a diagonal, rather than a full, complex block. The μ-value and H_∞ norm are equivalent only when the uncertain block Δ is a full complex matrix. This difference implies that in the dual-stage case, we cannot use the full 2 by 2 Δ block to set the H_∞ norm bound. Instead, the H_∞ norm bound for each uncertain channel (Δ_V and Δ_M) is set first, then a tighter upper bound, which is strictly less than 1, is assigned to the H_∞ norm of each uncertainty channel so that the constraint (11) is still satisfied.

3) Multi-objective optimization via LMI: From the above discussion, we have shown that the controller design of a track-following servo may be cast as an H_2 norm optimization problem with some H_∞ norm constraints, that is, given the general plant P, we want to design an output dynamic feedback controller such that

$$\mathcal{C} = \arg\min_{\mathcal{C}} \gamma_2\,, \tag{12}$$

$$\text{with} \quad \|G_{z_2w_2}\|_2 < \gamma_2\,, \tag{13}$$

$$\|G_{\Delta_V}\|_\infty < \gamma_V\,, \tag{14}$$

$$\text{and} \quad \|G_{\Delta_M}\|_\infty < \gamma_M\,. \tag{15}$$

Now the problem can be cast into a standard mixed-norm optimization problem. With the aid of the LMI-toolbox in MATLAB [12] and a highly efficient LMI solver SeDuMi [13], this problem is readily solved and synthesized.

III. Design and Simulation Results

In this design, the PES is sampled at 25 kHz. As mentioned before, this sampling rate is limited by the disk drive hardware configuration and cannot be increased arbitrarily, while the y_{RPES} and y_{PZT} are sampled at 50 kHz so as to effectively compensate airflow induced vibration of high frequency resonance modes. The resulting tracking controller is a double-input-double-output dynamic system that has the same order as the generalized plant, which is of order 21. A lower order controller is always preferred in order to reduce the computational time which in turn results in less controller delay during the controller implementation. Time delay not only deteriorates system performance, but also makes it less stable. In this design, the Hankel model reduction technique [11] is applied to the designed controller and the order of the final controller has been reduced from 21 to 14, without a noticeable performance deterioration.

A. Dynamics of the Tracking Controller

For illustration purposes, the dynamics of the reduced-order controller from the PES to VCM control input, u_v, for weight set (a) is shown in Fig. 7. Three controllers are considered: the first achieves H_2 norm minimization only, which is equivalent to the standard LQG design; the second achieves H_2 norm minimization under H_∞ norm constraints

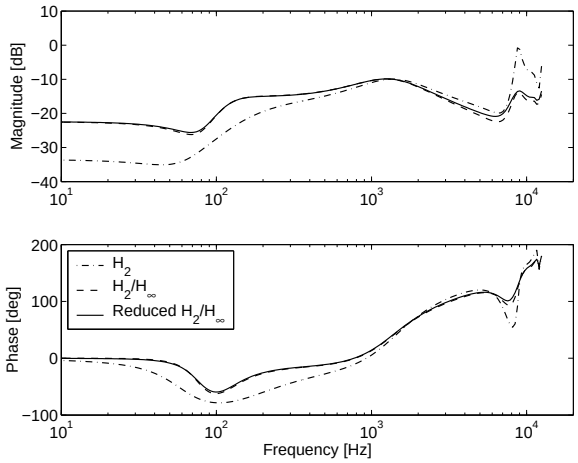

Fig. 7. Bode plots of various controllers

while the third is the reduced-order version of the second controller.

From Fig. 7, it can be seen that the H_2 controller has multiple peaks and notches, especially in the high frequency range. These fine features are introduced by the mode shapes of the actuator dynamics, disturbance weighting functions and uncertainty weighting functions. These features are expected to shape the controller dynamics in such a way that the best tracking performance is achieved, i.e., the RMS value of PES is minimized. However, system stability robustness is not guaranteed. When H_∞ bounds are imposed on the controller design process to guarantee robust stability, those high frequency peaks corresponding to actuator modes are greatly lowered, in order to attain more robustness when modelling uncertainties become large in the high frequency range.

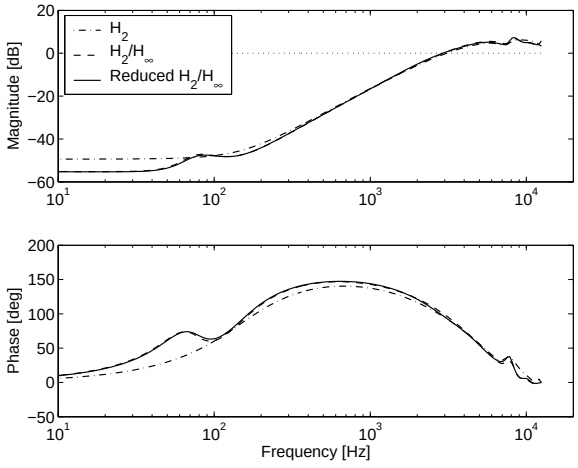

Fig. 8. Bode plots of sensitivity transfer functions resulting from three controller designs

Fig. 8 shows the Bode plots of sensitivity transfer functions resulting from the three controllers mentioned above. The bandwidths for these systems are about 3 kHz. These curves are almost the same except in the low frequency range. Note that those sensitivity functions do not reflect the vibration attenuation effect in the inner loop, since structural vibrations are mainly excited by airflow turbulence rather than by the track runout, and they are already handled by the inner loop vibration damping and compensation controller.

B. Robust Stability Analysis

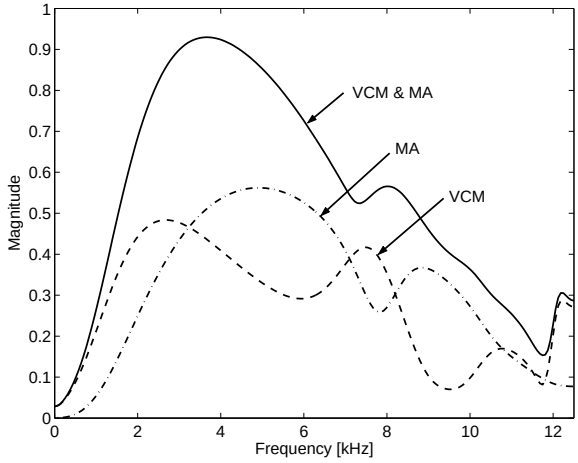

Fig. 9. Stability μ-values for different multiplicative uncertainty channels.

μ-value plots of the feedback system for either the individual or combined effect of the uncertainties Δ_V and Δ_M are shown in Fig. 9. As shown in the figure, when the two uncertainty channels take effect simultaneously, the resulting μ-value (solid curve) is roughly the summation the μ values that result when each uncertainty channel acts individually. Since the magnitude of overall μ plot is always less than one, the closed-loop system is robustly stable under the presumed multiplicative uncertainties. The results also explain why a tighter H_∞ bound should be assigned to each uncertainty channel, so that the final closed-loop system could still remain stable even when both uncertainty channels take effect simultaneously.

Although it is infeasible to use parametric uncertainties at the controller syntesis stage, using the control design methodology presented in this paper, it is possible to analyze the controller's stability robustness to parametric uncertainties after it has been designed. Consider a single resonance mode defined by

$$G(s) = \frac{b}{s^2 + a_1 s + a_0}\,, \tag{16}$$

where a_0, a_1 and b are the parameters corresponding to the natural frequency, damping factor, and modal constant of that mode. By assuming certain percentage of variation for each parameter, a linear fractional transformation (LFT) representation of the variations in these three parameters can easily be derived [11] with the diagonal uncertainty matrix, Δ, defined by $\Delta := \mathrm{diag}([\delta_{a_0}\, \delta_{a_1}\, \delta_b])$. The three normalized real parameters in Δ represent relative variations of their corresponding parameters.

TABLE I

PARAMETER VARIATIONS OF RESONANCE MODES (i=1,2,3).

Parameter	Variation
VCM natural frequency ($\sqrt{a_{i0}}$)	10 %
MA natural frequency ($\sqrt{a_0}$)	15 %
Damping factor (a_{i1}, a_1)	20 %
Modal constant (b_i, b)	5 %

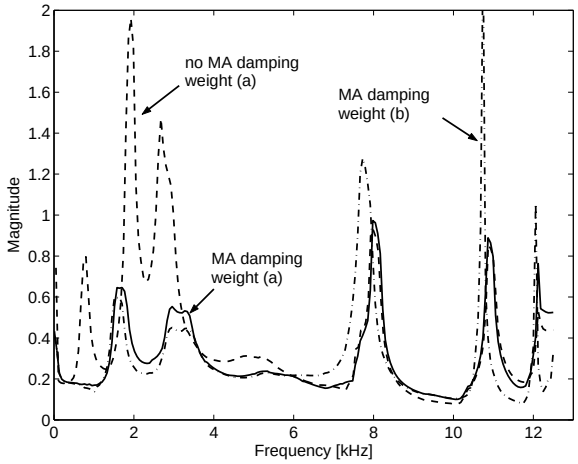

Fig. 10. Stability μ-values for parameter uncertainties.

In this analysis, parameter variations in the uncertain dual-stage actuator model are shown in Tab. I. The subscript i denotes the three major off-track modes of the model, which includes modes in the E-block and suspension. A bigger variation ($\pm 15\%$) is assumed for the MEMS MA resonance mode, which is due to lithographic misalignment and variations present in etching processes. The resulting μ-plots are shown in Fig. (10). From the stability μ-plot, we can see that, when the $RPES$ MA minor loop is used, the closed-loop system retains its stability under the parameter variations shown in Tab. I. Without the MA minor loop, the peaks due to MA parameter variations are much higher. A recalculation shows that if the MA minor loop is not used, the resulting control system can only withstand a variation of $\pm 8\%$ in MA natural frequency. This deterioration partially results from the gap between the representations of multiplicative and parametric uncertainties. The difference between the weight sets (a) and (b) in the robust stability of the inner loop vibration control is also shown in the figure. When the compensation effort of MA is increased, as in the case when weight set (b) is used, the closed-loop system tends to be less stable. This is partially due to the fact that the MA vibration compensation controller is primarily based on a feedforward compensation motion, which is generally more sensitive to parameter variations than feedback compensation.

C. Track-Following Performance

The designed system was simulated in time domain using more realistic disturbance sequences such as track runout, airflow turbulence. For comparison, a single-rate track-following controller was designed without inner loop vibration damping and compensation control. The RMS value of the position error signal, PES, is 4.44 nm and 5.31 nm, respectively, showing an improvement in tracking performance by about 17%. This improvement is mainly due to the fact that a higher rate is used for the inner loop vibration control while the outer loop tracking controller runs at only 25 kHz, which is not adequate for coping with high frequency structural vibrations.

IV. CONCLUSION

In this paper, a dual-stage track-following controller is designed based on the multi-objective optimization method. Various closed-loop system specifications, such as minimization of the RMS of PES, and robust stability, were cast into a set of LMIs with controller parametrization. The robust stability criterion for the dual-stage system is adapted such that the multi-channel μ-value constraint can still be satisfied. Simulation results show that the designed controller can achieve better tracking performance, as compared to a previously designed controller that was designed with the sensitivity decoupling method [3], while stability robustness is still maintained under assumed multiplicative and parametric uncertainties. Future work involves experimental verifications which will be done after the MEMS MA and instrumented suspension are fabricated and integrated.

REFERENCES

[1] S. Koganezawa, Y. Uematsu, and T. Yamada, "Dual-stage actuator system for magnetic disk drives using a shear mode piezoelectric microactuator," *IEEE Trans. Magnetics*, vol. 35, pp. 988–992, 1999.

[2] S. J. Schroeck and W. C. Messner, "On controller design for linear time-invariant dual-input single-output systems," in *Proc. Amer. Control Conf.*, 1999, pp. 4122–4126.

[3] Y. Li and R. Horowitz, "Mechatronics of electrostatic microactuators for computer disk drive dual-stage servo systems," *IEEE/ASME Trans. Mechatronics*, vol. 6, no. 2, pp. 111–121, 2001.

[4] X. Hu, W. Guo, T. Huang, and B. M. Chen, "Discrete-time LQG/LTR dual-stage controller design and implementation for high track density hdds," in *Proc. Amer. Control Conf.*, 1999, pp. 4111–4115.

[5] Y. Li and R. Horowitz, "Design and testing of track-following controllers for dual-stage servo systems with pzt actuated suspensions," *Microsystem Technologies*, vol. 8, pp. 194–205, 2002.

[6] D. H. Shim, H. S. Lee, and L. Guo, "Mixed-objective optimization of track-following controllers using linear matrix inequalities," in *Proc. of Amer. Control Conf.*, vol. 3, 2003.

[7] M. C. D. Oliveira, J. C. Geromel, and J. Bernussou, "Extended H_2 and H_∞ norm characterizations and controller parametrizations for discrete-time systems," *Int. J. Control*, vol. 75, no. 9, pp. 666–679, 2002.

[8] C. W. Scherer and S. Weiland, *Lecture Notes DISC Course on LMI in Control*, 2nd ed., 1999.

[9] Y. Huang, M. Banther, P. D. Mathur, and W. Messner, "Design and analysis of a high bandwidth disk drive servo system using an instrumeted suspension," *IEEE/ASME Trans. Mechatronics*, vol. 4, no. 2, pp. 196–206, 1999.

[10] Y. Li, F. Marcassa, R. Horowitz, R. Oboe, and R. Evans, "Track-following control with active vibration damping of a PZT-actuated suspension dual-stage servo system," in *Proc. of Amer. Control Conf.*, vol. 3, 2003.

[11] G. J. Balas, J. C. Doyle, K. Glover, A. Packard, and R. Smith, *μ-Analysis and Synthesis Toolbox for use with MATLAB.* MUSYN Inc. and The MathWorks, Inc., USA, 1995.

[12] P. Gahinet, A. Nemirovske, A. J. Laub, and M. Chilali, *LMI Control Toolbox*. The MathWorks, Inc., USA, 1995.

[13] J. F. Sturm, *Using Sedumi 1.05, A MATLAB Toolbox for Optimization over Symmetric Cones*, 2001.